Chemical Science

ROYAL SOCIETY OF CHEMISTRY

EDGE ARTICLE

View Article Online
View Journal | View Issue

Cite this: *Chem. Sci.*, 2026, **17**, 7958

All publication charges for this article have been paid for by the Royal Society of Chemistry

Received 29th January 2026
Accepted 18th February 2026

DOI: 10.1039/d6sc00802j

rsc.li/chemical-science

Pnictogen-bonding-crosslinked polymer networks: constructing self-healing materials

Qingli Song,[a] Yi Liu,[b] Yao Wang *[b] and Wei Wang *[ac]

Herein, we introduce pnictogen bonding interaction into polymer networks for the design and modulation of dynamic macromolecular materials. Several types of polymeric pnictogen-bonding networks with graded interaction strengths were constructed to explore the structure–property relationship. Comprehensive investigations revealed that strengthening the pnictogen bonding significantly enhances the topological stability of the resulting materials. In contrast, analogous hydrogen-bonded networks did not exhibit comparable mechanical reinforcement. Moreover, the pnictogen-bonding networks endow the materials with tunable self-healing capability, allowing not only spontaneous healing at room temperature and thermally triggered healing on demand, but also effective healing in aqueous environments. This represents the first exploration of self-healing behavior driven by pnictogen bonding in polymeric materials. Mechanistic insights into the role of pnictogen bonding in polymer networks were elucidated through NMR titration of donor–acceptor polymer pairs, comparative self-assembly behavior, and cocrystal structures of small-molecule analogues. The incorporation of pnictogen bonding interaction into polymer networks provides a robust and versatile platform for engineering high-performance dynamic polymeric materials.

Introduction

Crosslinking between polymer chains enables the construction of polymer networks (PNs) with distinct mechanical and functional properties. PNs formed *via* permanent covalent bonds exhibit excellent strength and durability; however, the irreversible nature of these crosslinks restricts molecular-level rearrangement, thereby precluding self-healing and reprocessability.[1] In contrast, dynamically crosslinked PNs based on reversible bonds offer topological adaptability, allowing bond exchange under specific stimuli. This dynamic behavior imparts viscoelasticity that bridges solid-like and liquid-like characteristics, and translates macroscopically into intelligent functions such as self-healing, shape reconfiguration, and stimulus responsiveness.[2] Dynamically crosslinked PNs are broadly classified into covalent and non-covalent types. Dynamic covalent PNs, the most extensively studied class,[3] utilize reversible covalent reactions (*e.g.*, Diels–Alder cycloaddition,[4] disulfide exchange,[5] transesterification,[6] and imine exchange[7]) to enable network rearrangement. Although dynamic covalent PNs exhibit superior mechanical robustness, the inherently slow dissociation kinetics of dynamic covalent bonds often lead to sluggish responses under mild, catalyst-free conditions. Conversely, non-covalent bonds typically possess lower bond energies and faster dissociation kinetics. These attributes facilitate rapid network reorganization under benign conditions without catalysts, endowing materials with exceptional intrinsic self-healing capabilities while typically resulting in compromised mechanical strength.[8]

A wide range of supramolecular interactions, including hydrogen bonding,[9] host–guest interactions,[10] ionic interactions,[11] π–π stacking,[12] van der Waals forces,[13] and coordination interactions involving metal centers[14] or boron-based compounds,[15] have been exploited to construct dynamic PNs. Among these, hydrogen-bonded polymer networks (HB-PNs) based on donor–acceptor motifs are the most extensively studied.[16] However, hydrogen bonding suffers from several intrinsic limitations, including the generally weak strength of monodentate interactions, poor tolerance toward polar solvents,[17] and design constraints imposed by the hard–soft acid–base (HSAB) principle, which restrict the incorporation of soft acceptors into dynamic PNs.[18]

To address these limitations, nonclassical weak interactions such as halogen bonding (XB) and chalcogen bonding (ChB) have emerged as alternative supramolecular motifs for dynamic polymeric materials (Fig. 1a–b). For example, Schubert and co-workers pioneered the construction of monovalent halogen-bonded polymer networks using polymeric iodo-triazole donors and carboxylate acceptors, which exhibited self-

[a]*Department of Chemistry, Zhengzhou University, Zhengzhou 450001, China. E-mail: wangwei_chem@zzu.edu.cn*

[b]*School of Chemistry and Chemical Engineering, Key Laboratory of the Colloid and Interface Chemistry, Ministry of Education, Shandong University, Jinan, 250100, China. E-mail: yaowang@sdu.edu.cn*

[c]*Shenzhen Research Institute of Shandong University, A301 Virtual University Park in South District of Shenzhen, China*

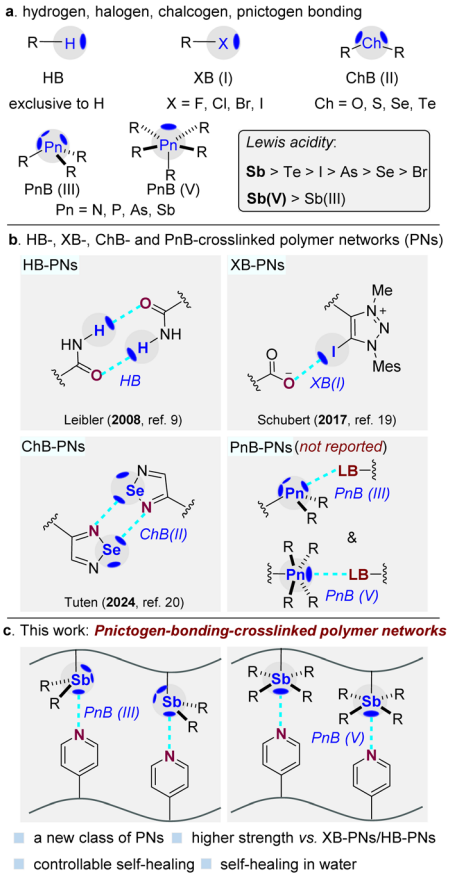

Fig. 1 (a) Hydrogen, halogen, chalcogen, and pnictogen bonding (HB, XB, ChB and PnB). (b) HB-, XB-, ChB- and PnB-crosslinked polymer networks. (c) Pnictogen-bonding-crosslinked polymer networks (PnB-PNs).

healing behavior at elevated temperatures.[19] Tuten and Puttreddy independently employed selenadiazole motifs as donors and acceptors to construct divalent chalcogen-bonded polymer networks, endowing the resulting materials with self-healing and shape-memory properties.[20,21] Despite these important advances, it remains challenging to identify supramolecular interactions that simultaneously offer strong and tunable binding while maintaining rapid reversibility, a prerequisite for bridging the gap between weak noncovalent interactions and irreversible covalent crosslinks in dynamic PNs.

Pnictogen bonding (PnB) has recently emerged as a distinctive noncovalent interaction in supramolecular chemistry.[22] Compared with HB, XB, and ChB, PnB donors typically possess multiple accessible σ-holes, enabling enhanced binding directionality and increased structural complexity (Fig. 1a). In addition, systematic variations in donor polarizability and electronegativity lead to a characteristic trend in Lewis acidity (Sb > Te > I > As > Se > Br),[22a] suggesting that antimony-based donors can form particularly strong yet directional supramolecular interactions. These features render PnB a promising, yet unexplored, motif for constructing robust dynamic polymer networks, especially for regulating macroscopic properties such as self-healing behavior.

Herein, we report the first pnictogen-bonding-crosslinked polymer networks (PnB-PNs) (Fig. 1c). By exploiting directional interactions between electrophilic Sb(III/V) centers and pyridine-functionalized polymer chains, efficient and reversible interchain crosslinking is achieved. Systematic modulation of pnictogen-bonding strength reveals clear correlations between supramolecular interaction strength, network topology, and dynamic material properties, establishing PnB as a versatile platform for the rational design of high-performance dynamic polymeric materials.

Results and discussion

To unequivocally demonstrate the feasibility of constructing PnB-PNs while eliminating potential interferences (*e.g.*, ionic electrostatic interactions and hydrogen bonding involving labile protons), we designed a series of derivatives based on a neutral styrenic backbone lacking both heteroatoms and active hydrogen atoms (Fig. 2a). To minimize structural variations among PnB donors, monomers **1** (P-centered) and **2** (Sb-centered), featuring identical molecular frameworks, were synthesized. In addition, monomer **3** incorporating Sb(v) was prepared to examine the influence of antimony oxidation state on network properties. Computational analyses were conducted to preliminarily assess the PnB donor strength. Electrostatic potential (ESP) mapping revealed three well-defined σ-holes in the tetrahedral geometries of monomers **1** and **2**, with monomer **2** exhibiting markedly higher maximum positive ESP values than monomer **1**, indicative of its enhanced PnB donor strength

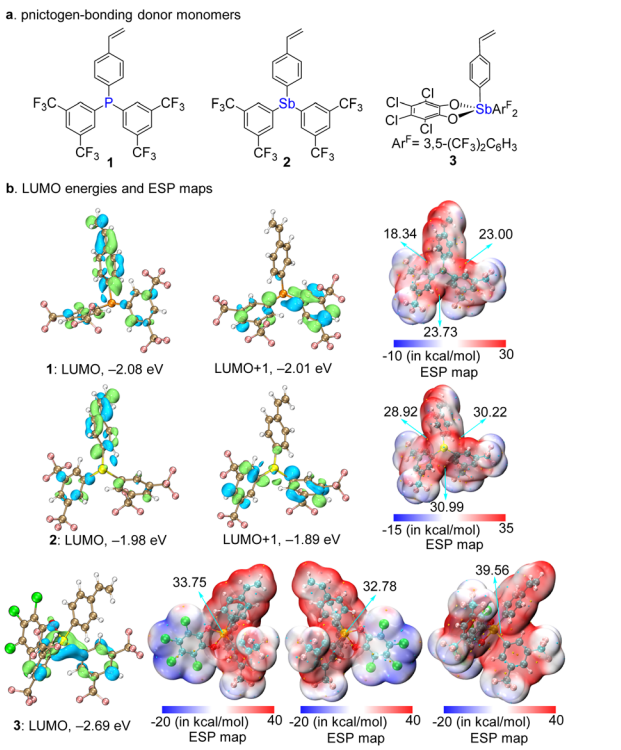

Fig. 2 (a) PnB donor monomers. (b) LUMO energies and ESP maps of **1**, **2** and **3**.

(Fig. 2b). This increase can be attributed to the higher polarizability and lower electronegativity of Sb relative to P. In contrast, monomer **3**, with a high-valent Sb center, shows a further enhancement of the σ-hole, reflecting its intrinsically stronger Lewis acidity. In addition to the electrostatic analysis, LUMO energy calculations show that monomer **3** possesses a substantially lower LUMO energy than both **1** and **2**, suggesting a significantly enhanced ability to accept electron density from Lewis bases. Taken together, the combined ESP and LUMO analyses establish a clear trend in the PnB donor strength of **3** > **2** > **1** when interacting with the same acceptor, consistent with the expected Lewis acidity order of Sb(v) > Sb(III) > P(III).[22b]

Guided by computational predictions of PnB donor strength, we initially pursued the synthesis of polymeric PnB donors *via* copolymerization of monomers **1–3** separately with styrene. This approach successfully afforded copolymers **P1** and **P2** from monomers **1** and **2**, respectively (Fig. 3a). However, attempts to polymerize monomer **3** led to complex product mixtures, likely due to decomposition of the high-valent Sb(v) centers under radical polymerization conditions. To overcome this limitation, a post-polymerization modification strategy was employed. Precursor polymer **P2** was treated with 3,4,5,6-tetrachlorocyclohexa-3,5-diene-1,2-dione to efficiently generate the Sb(v)-based polymeric donor **P3**. In parallel, the PnB acceptor polymer was synthesized by RAFT copolymerization of pyridyl methacrylate with butyl acrylate. All copolymers were thoroughly characterized by NMR spectroscopy and elemental microanalysis, confirming their chemical structures. Size exclusion chromatography (SEC) revealed number-average molecular weights (M_n) of approximately 13 000 g mol^{-1} for the target polymers.

To date, no macromolecular pnictogen-bonding polymers have been reported, and thus direct observation of PnB interactions between polymeric donors and acceptors has remained elusive. To investigate such interactions, we performed solution-phase ^{1}H NMR titration experiments. In CD_2Cl_2, no appreciable chemical shift changes were detected for donor protons in the **P1**/**P4** and **P2**/**P4** systems, even at donor-to-acceptor molar ratios of up to 1 : 10 (Fig. S1 and S3 in the SI), indicating either intrinsically weak binding or the limited detection sensitivity of ^{1}H NMR. In stark contrast, the Sb(v)-based polymeric donor **P3** exhibited pronounced chemical shift perturbations upon titration with acceptor polymer **P4** (Fig. S5 in the SI). Incremental addition of **P4** induced progressive upfield shifts in the diagnostic **P3** proton signals (H^1 and H^2), consistent with specific intermolecular interactions (Fig. 3b). In addition, ^{1}H NMR titration experiments were conducted for the PnB monomer **3** with the Lewis base monomer **M2**, revealing a similar trend in proton chemical shift changes (Fig. S9 in the SI). Nonlinear regression analysis based on a 1 : 1 binding model afforded binding constants of $K_{(\mathbf{P3/P4})} = 1.57 \times 10^4$ M^{-1} and $K_{(\mathbf{3/M2})} = 0.69 \times 10^4$ M^{-1}. The substantially larger binding constant observed for the **P3**/**P4** system suggests that the presence of polymer chains promotes PnB donor–acceptor interactions, a phenomenon that has also been observed in XB polymer systems.[23]

To further assess the relative strengths of PnB interactions in the **P1**/**P4**, **P2**/**P4**, and **P3**/**P4** systems, the more sensitive ^{13}C NMR technique was employed to monitor intermolecular interactions between the polymers. Equimolar mixtures of the polymeric acceptor **P4** with the polymeric donors **P1–P3** were subjected to comparative ^{13}C NMR analyses. As a result, pronounced upfield shifts of the pyridine C_2 carbon resonance were observed for the **P2**/**P4** and **P3**/**P4** systems, amounting to 0.52 and 4.33 ppm, respectively, whereas only negligible changes were detected for the **P1**/**P4** system (Fig. 3c). These results clearly establish an interaction strength hierarchy of **P3**/**P4** > **P2**/**P4** >> **P1**/**P4**. Notably, no discernible chemical shift changes were detected for the ester carbonyl signals in any of

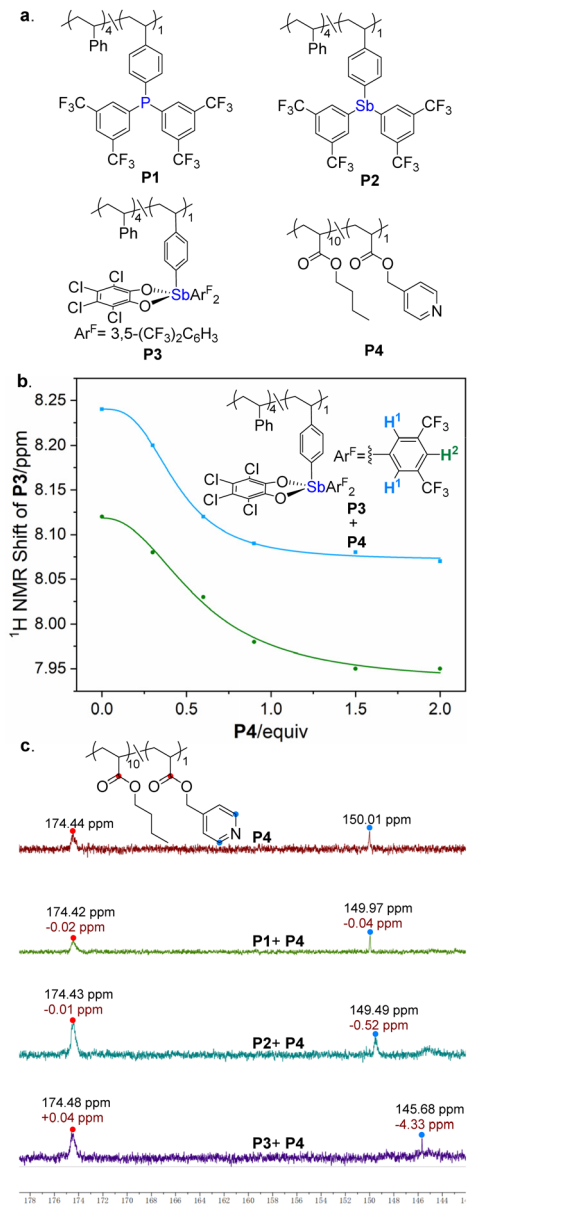

Fig. 3 (a) Polymeric PnB donors and acceptors. (b) ^{1}H NMR titration curves of PnB donor polymer **P3** (0.01 M) and PnB acceptor polymer **P4**. (c) ^{13}C NMR analysis of PnB interaction strengths (PnB donor and acceptor, both 0.01 M).

the three systems, indicating that the pyridine moiety of **P4** preferentially participates in PnB formation rather than the ester carbonyl group. This observation is fully consistent with the original molecular design.

Having established a PnB strength hierarchy of **P3**/**P4** > **P2**/**P4** >> **P1**/**P4**, we next examined the self-assembly behavior of these systems in solution. Owing to the hydrophobic nature of the polymers, assembly was induced by the gradual addition of water to THF solutions containing equimolar amounts of the PnB donor and acceptor components. Notably, distinct assembly behaviors were observed. Whereas the **P2**/**P4** and **P3**/**P4** systems formed translucent, gel-like solutions, the **P1**/**P4** mixture remained a clear solution (Fig. 4a–c). Transmission electron microscopy (TEM) further revealed well-defined spherical nanostructures in the **P2**/**P4** and **P3**/**P4** systems, while no discernible assemblies were detected for **P1**/**P4** (Fig. 4a–c). Consistent with these observations, dynamic light scattering (DLS) measurements revealed that the **P2**/**P4** and **P3**/**P4** systems formed nanoscale aggregates with average apparent hydrodynamic diameters of 111 nm ($\sigma = 52$ nm) and 118 nm ($\sigma = 44$ nm), respectively, whereas the **P1**/**P4** system displayed a much smaller hydrodynamic diameter of only 5.3 nm ($\sigma = 1.7$ nm), indicative of the absence of significant aggregation (Fig. 4d). Collectively, these results indicate that pronounced PnB interactions in the **P2**/**P4** and **P3**/**P4** systems effectively promote supramolecular organization, whereas the absence of significant **PnB** interactions in the **P1**/**P4** system is insufficient to drive self-assembly.

Having clarified the solution-state binding behavior of the polymeric donor–acceptor systems, we turned our attention to elucidating the relationship between PnB-PNs and the properties of dynamic materials. Polymer networks **P^{III}-PNs** (**P1**/**P4**), **Sb^{III}-PNs** (**P2**/**P4**), and **Sb^{V}-PNs** (**P3**/**P4**) were fabricated *via* solvent evaporation from $CHCl_3$ solutions containing equimolar amounts of donor and acceptor units (Table 1). To examine chain-length effects, an additional Sb(III)-based network (**Sb^{III}-PNs′**) was fabricated using **P2** and a longer acceptor polymer **P4′** with an M_n approximately 2.3 times that of

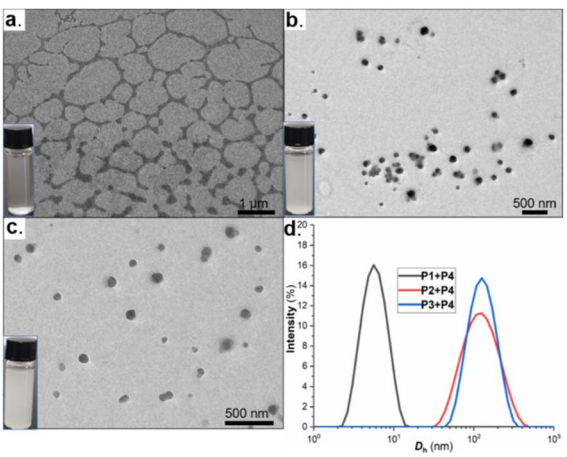

Fig. 4 (a–c) TEM images of the P1/P4, P2/P4, and P3/P4 assemblies. (d) Size distribution histogram of the three systems.

Table 1 Composition of the PNs and its corresponding glass transition temperature (T_g)

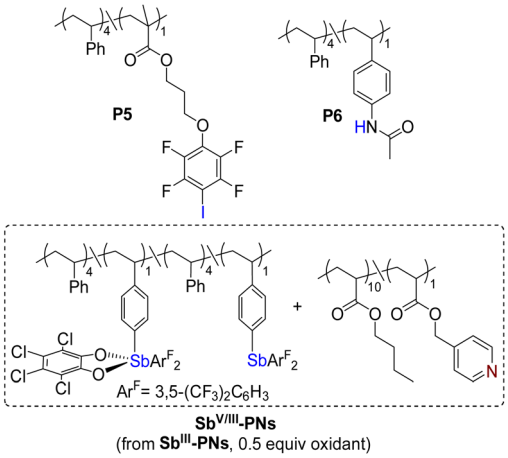

Entry[a]	PNs	Donors	Acceptors	T_g [°C]
1	**P^{III}-PNs**	**P1**	**P4**	−33
2	**Sb^{III}-PNs**	**P2**	**P4**	−19
3	**Sb^{III}-PNs′**	**P2**	**P4′**	−12
4	**Sb$^{V/III}$-PNs**	—	—	−14
5	**Sb^{V}-PNs**	**P3**	**P4**	9
6	**XB-PNs**	**P5**	**P4**	−35
7	**HB-PNs**	**P6**	**P4**	−37

[a] See the SI for details.

P4. Furthermore, a hybrid network (**Sb$^{V/III}$-PNs**) incorporating Sb(v) and Sb(III) donors in a 1 : 1 ratio was constructed to specifically assess the influence of high-valent Sb centers on network dynamics. For comparison, halogen-bonded (**XB-PNs**) and hydrogen-bonded (**HB-PNs**) polymer networks were prepared under analogous conditions.

Differential scanning calorimetry (DSC) revealed a clear correlation between PnB strength and thermal properties. The Sb(III)-based network **Sb^{III}-PNs** exhibited a higher glass transition temperature ($T_g = -19$ °C) than the P(III)-based **P^{III}-PNs** ($T_g = -33$ °C) (Fig. S19 and S20), consistent with stronger Sb···N interactions imposing greater constraints on polymer chain mobility. Increasing the acceptor chain length further elevated the T_g of **Sb^{III}-PNs′** to −12 °C, likely due to enhanced chain entanglement. Notably, incorporation of Sb(v)-based PnB interactions led to a further increase in T_g, with values of −14 °C for **Sb$^{V/III}$-PNs** and 9 °C for **Sb^{V}-PNs**, reflecting the superior bonding capability of Sb(v) and the resulting enhancement in network rigidity. In contrast, **XB-PNs** and **HB-PNs** displayed substantially lower T_g values (−35 °C and −37 °C, respectively), indicating their comparatively limited topological stability.

To further explore the mechanical implications of PnB, we conducted qualitative vial creep experiments to assess the dimensional stability of these PNs (Fig. 5a). Notably, **Sb^{III}-PNs′**, **Sb^{V}-PNs** and **Sb$^{V/III}$-PNs** exhibited excellent shape retention, with no visible deformation under the applied conditions. In comparison, **Sb^{III}-PNs** exhibited only minor distortion, whereas

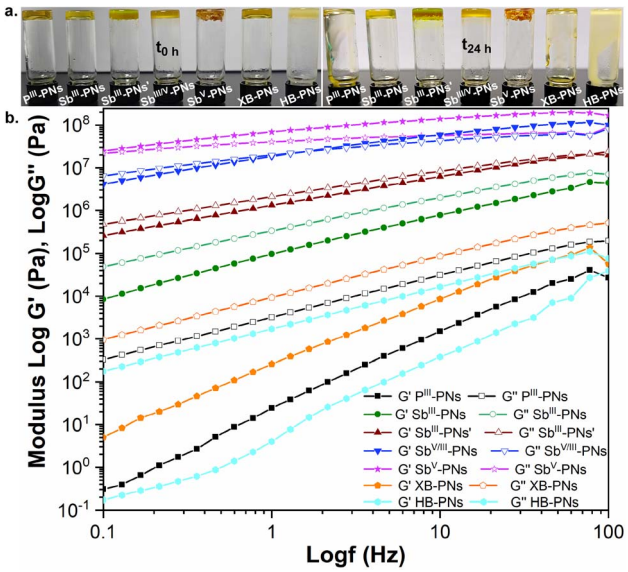

Fig. 5 (a) Vial creep experiments. (b) Rheological experiments.

P^{III}-PNs, **XB-PNs**, and **HB-PNs** all underwent pronounced creep deformation.

Complementary oscillatory shear rheological measurements were conducted to elucidate the influence of PnB on the viscoelastic properties of crosslinked polymer networks (Fig. 5b). At room temperature, both **P^{III}-PNs** and **Sb^{III}-PNs** exhibited loss moduli (G'') exceeding their storage moduli (G'), characteristic of viscoelastic liquid-like behavior. Compared to **P^{III}-PNs**, **Sb^{III}-PNs** displayed substantially higher moduli and a smaller G''–G' gap, indicating enhanced structural rigidity arising from stronger crosslinking interactions. Incorporation of longer acceptor polymer chains in **Sb^{III}-PNs′** further increased the moduli and narrowed the G''–G' gap. The introduction of Sb(v)-based PnB led to a further enhancement in mechanical strength: **Sb$^{V/III}$-PNs** and **Sb^{V}-PNs** exhibited progressively higher moduli, with **Sb^{V}-PNs** displaying $G' > G''$, indicative of dominant elastic behavior. In contrast, **XB-PNs** and **HB-PNs** showed rheological responses comparable to those of **P^{III}-PNs**.

To quantitatively correlate network mechanics with the bond strength of PnB, creep-recovery experiments were performed under constant stress (1000 Pa, 1000 s) (Table 2, Fig. S31–S39 in the SI). **P^{III}-PNs**, **XB-PNs**, and **HB-PNs** exhibited large irreversible strains of 202 700%, 67 020%, and 375 500%, respectively, indicative of weak network cohesion and poor mechanical robustness. By comparison, **Sb^{III}-PNs** displayed a substantially reduced deformation of 1856%, reflecting enhanced structural integrity. Notably, extension of the acceptor polymer chains further suppressed creep deformation, as evidenced by a markedly lower strain of 84.16% for **Sb^{III}-PNs′**. In sharp contrast, networks incorporating stronger Sb(v)–PnB interactions exhibited dramatically improved resistance to creep, with strains of only 1.72% for the Sb(III)/Sb(v) hybrid **Sb$^{V/III}$-PNs** and an exceptionally low 0.11% for the pure Sb(v)-based **Sb^{V}-PNs**. Moreover, **Sb^{V}-PNs** maintained outstanding thermomechanical robustness at elevated temperature (60 °C), showing only 8.56% strain under identical testing conditions. Upon the addition of one equivalent of quinoline to **Sb^{V}-PNs**, the room-temperature creep strain increased from 0.11% to 18.74%, suggesting that quinoline acts as a competitive reagent that partially disrupts Sb(v)–PnB interactions and thereby weakens the polymer network.

Motivated by the pronounced mechanical reinforcement conferred by Sb-based PnB in dynamic materials, films of **Sb^{III}-PNs**, **Sb^{III}-PNs′**, **Sb$^{V/III}$-PNs** and **Sb^{V}-PNs** were prepared to systematically investigate the influence of PnB on self-healing behavior in dynamic polymer networks. Notably, the Sb(III)-based networks **Sb^{III}-PNs** and **Sb^{III}-PNs′** exhibited excellent room-temperature self-healing, achieving complete notch closure within 5 h and 12 h, respectively (Fig. 6a–d). In contrast,

Table 2 Strains of PNs under constant stress (1000 Pa, 1000 s)

Entry[a]	PNs	Temperature [°C]	Strain [%]
1	**P^{III}-PNs**	25	202 700
2	**Sb^{III}-PNs**	25	1856
3	**Sb^{III}-PNs′**	25	84.16
4	**Sb$^{V/III}$-PNs**	25	1.72
5	**Sb^{V}-PNs**	25	0.11
6	**Sb^{V}-PNs**	60	8.56
7	**Sb^{V}-PNs** + quinoline	25	18.74
8	**XB-PNs**	25	67 020
9	**HB-PNs**	25	375 500

[a] See the SI for details.

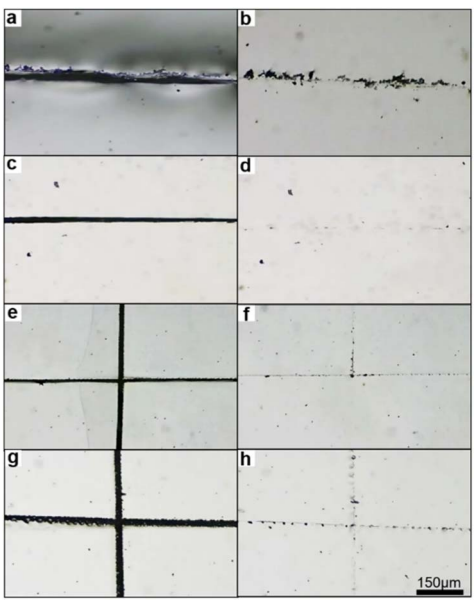

Fig. 6 (a) Optical micrographs of the damaged film Sb^{III}-PNs. (b) Optical micrographs of the film Sb^{III}-PNs after healing for 5 h at room temperature. (c) Optical micrographs of the damaged film Sb^{III}-PNs′. (d) Optical micrographs of the film Sb^{III}-PNs′ after healing for 12 h at room temperature. (e) Optical micrographs of the damaged film Sb$^{V/III}$-PNs. (f) Optical micrographs of the film Sb$^{V/III}$-PNs after healing for 20 h at room temperature. (g) Optical micrographs of the damaged film Sb^{V}-PNs. (h) Optical micrographs of the film Sb^{V}-PNs after healing for 24 h at 60 °C.

the stronger Sb(v)–PnB interactions reduced healing efficiency, since the Sb(v)/Sb(iii) hybrid **Sb$^{V/III}$-PNs** required 20 h at room temperature to reach a similar degree of healing (Fig. 6e–f). Remarkably, **Sb^{V}-PNs** exhibited effective healing only at elevated temperature (60 °C) (Fig. 6g–h). This inverse relationship between healing kinetics and pnictogen-bonding strength is attributed to the restricted chain mobility imposed by stronger PnB interactions at damaged interfaces, which hinders effective contact and reorganization of donor and acceptor moieties. As a result, additional thermal energy is necessary to overcome activation barriers associated with chain diffusion and dynamic bond exchange.

Given that Sb(v)–PnB in polymer networks exhibit markedly stronger constraints on chain mobility than their Sb(iii) counterparts, a quantitative analysis of the exchange kinetics of these two dynamic bonds is essential. Such polymer networks display frequency-dependent mechanical behavior characterized by a single crossover frequency separating the elastic-dominated and viscous-dominated regimes. This crossover frequency corresponds to the inverse of the terminal relaxation time (τ), which represents the average timescale for network reconfiguration and can be regarded as the effective bond lifetime.[24] The shear modulus spectra of **Sb^{III}-PNs** and **Sb^{V}-PNs** were measured at 20 °C, affording terminal relaxation times (τ) of 3.72 ms and 45.15 s, respectively (Fig. S40–S41 in the SI). This more than four-orders-of-magnitude increase in τ directly evidences a dramatically slower network reconfiguration and severely restricted chain mobility in the Sb(v)-based networks. To further elucidate the kinetic origin of this disparity, temperature-dependent shear modulus measurements were performed to track the evolution of τ and to extract the corresponding relaxation activation energies (E_a).[25] **Sb^{V}-PNs** exhibit a substantially higher E_a than **Sb^{III}-PNs** (240 kJ mol^{-1} *versus* 166 kJ mol^{-1}), indicating a much larger energetic barrier for chain diffusion and dynamic bond exchange. The unusually large activation energy of **Sb^{V}-PNs** implies a pronounced temperature sensitivity of chain dynamics, thereby rationalizing the necessity of elevated temperatures to enable efficient self-healing.

Building on the established relationship between pnictogen-bonding strength and healing efficiency, tensile testing was conducted on **Sb$^{V/III}$-PNs**, selected for its optimal balance of room temperature self-healing and mechanical performance (Fig. 7). The pristine specimen exhibited an ultimate tensile strength of 0.30 MPa and an elongation at break of 651%. Following complete sectioning to mimic material damage and subsequent intimate contact of the fracture surfaces, the sample was allowed to heal at room temperature for 24 hours. Post-healing tensile measurements demonstrated 90% recovery of the original strength (0.27 MPa) and 87% restoration of elongation at break (569%), confirming substantial mechanical recovery. This recovery correlates directly with the observed macroscopic healing of **Sb$^{V/III}$-PNs** films, confirming effective damage remediation under mild conditions.

Given that PnB constitutes a weak interaction with low sensitivity to polar solvents, this feature was expected to endow PnB-PNs with self-healing ability in aqueous environments. To verify this hypothesis, samples of **Sb$^{V/III}$-PNs** were completely cut, the freshly exposed surfaces were brought into intimate contact, and the specimens were immersed in water for 24 h at room temperature. Subsequent tensile tests under identical conditions to the pristine samples revealed that the mechanical parameters of specimens self-healed in water were comparable to those healed under ambient conditions (Fig. S47 in the SI). These findings confirm that the self-healing behavior of **Sb$^{V/III}$-PNs**-based dynamic materials is insensitive to aqueous environments.

Motivated by the robust polymer networks afforded by Sb(v)-based dynamic materials through strong PnB, we investigated the bonding modes between PnB donors and acceptors. The cocrystal of Sb(v)-based derivative **PnB^{V}** with pyridine was obtained *via* solvent diffusion using dichloromethane and *n*-hexane (Fig. 8). The crystal structure unambiguously reveals PnB interactions between the electrophilic antimony center in **PnB^{V}** and the nitrogen atom of pyridine. Key geometric parameters provide conclusive evidence: the Sb···N distance of

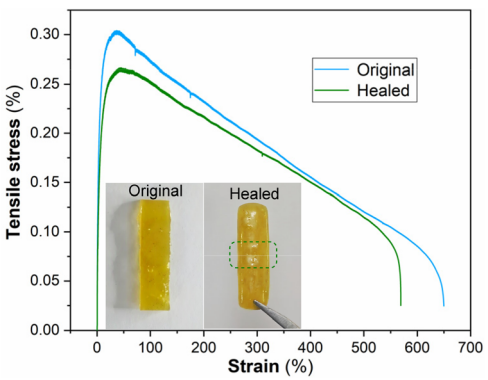

Fig. 7 The stress–strain curves of Sb$^{V/III}$-PNs before damage and after healing for 24 hours at room temperature.

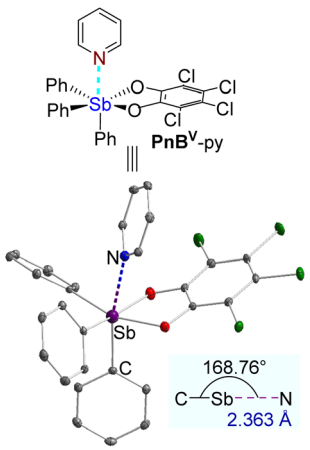

cocrystal structure of **PnB^{V}**-py
(hydrogen atoms were omitted for clarity)

Fig. 8 The cocrystal structure of PnB^{V}-py.

2.363 Å is markedly shorter than the sum of their van der Waals radii (3.65 Å), while the nearly linear C–Sb···N angle of 168.76° is characteristic of directional PnB. Furthermore, the Sb···N separation significantly exceeds typical covalent Sb–N bond lengths (~2.11 Å), thereby excluding the formation of coordinate covalent bonds. These structural data definitively validate the designed PnB interaction between Sb(v)-donor polymers and pyridine-functionalized acceptors.

Conclusions

In summary, polymer networks based on PnB have been established as a new platform for tuning the properties of dynamic materials. Several distinct crosslinked polymers featuring pnictogen-bonding motifs were synthesized, with ^{1}H NMR titration providing initial evidence of supramolecular interactions between polymeric PnB donors and acceptors. Notably, strengthening PnB within these polymer networks markedly enhances the topological stability, whereas comparable hydrogen-bonded systems exhibit negligible improvements. Moreover, Sb-based PnB-PNs exhibit tunable self-healing behavior, enabling on-demand switching between autonomous repair at ambient temperature and thermally triggered healing. Remarkably, the healing process can even be accomplished in aqueous environments. The complexation mode between polymeric donors and acceptors was further corroborated by cocrystal structures of model compounds. These findings highlight the significant potential of PnB-PNs for the design and development of next-generation dynamic materials.

Author contributions

W. W. and Y. W. conceived and designed the experiments. Q. S. conducted the experiments and prepared the supplementary materials. Y. L. performed DFT calculations. W. W. wrote the manuscript. All authors analysed the data, discussed the results and approved the manuscript.

Conflicts of interest

There are no conflicts to declare.

Data availability

CCDC 2480747 contains the supplementary crystallographic data for this paper.[26]

The data supporting this article have been included as part of the supplementary information (SI). Supplementary information: experimental details, spectroscopic data for the compounds, X-ray crystallographic details, and theoretical calculation details. See DOI: https://doi.org/10.1039/d6sc00802j.

Acknowledgements

We gratefully acknowledge the National Natural Science Foundation of China (22201160 and 22371169), the Natural Science Foundation of Henan Province (242301420057), the Natural Science Foundation of Guangdong Province (2021A1515110010), and the Postdoctoral Innovation Talent Support Program of Shandong Province (SDBX2020001).

Notes and references

1 R. Geyer, J. R. Jambeck and K. L. Law, Production, use, and fate of all plastics ever made, *Sci. Adv.*, 2017, **3**, e1700782.

2 (*a*) R. J. Wojtecki, M. A. Meador and S. J. Rowan, Using the dynamic bond to access macroscopically responsive structurally dynamic polymers, *Nat. Mater.*, 2011, **10**, 14–27; (*b*) N. Roy, B. Bruchmann and J.-M. Lehn, DYNAMERS: dynamic polymers as self-healing materials, *Chem. Soc. Rev.*, 2015, **44**, 3786–3807; (*c*) F. Van Lijsebetten, J. O. Holloway, J. M. Winne and F. E. Du Prez, Internal catalysis for dynamic covalent chemistry applications and polymer science, *Chem. Soc. Rev.*, 2020, **49**, 8425–8438.

3 Z. Lei, H. Chen, S. Huang, L. J. Wayment, Q. Xu and W. Zhang, New advances in covalent network polymers via dynamic covalent chemistry, *Chem. Rev.*, 2024, **124**, 7829–7906.

4 (*a*) X. Chen, M. A. Dam, K. Ono, A. Mal, H. Shen, S. R. Nutt, K. Sheran and F. Wudl, A thermally re-mendable cross-linked polymeric material, *Science*, 2002, **295**, 1698–1702; (*b*) T. F. Scott, A. D. Schneider, W. D. Cook and C. N. Bowman, Photoinduced plasticity in cross-linked polymers, *Science*, 2005, **308**, 1615–1617; (*c*) B. J. Adzima, H. A. Aguirre, C. J. Kloxin, T. F. Scott and C. N. Bowman, Rheological and chemical analysis of reverse gelation in a covalently cross-linked Diels–Alder polymer network, *Macromolecules*, 2008, **41**, 9112–9117.

5 (*a*) A. Rekondo, R. Martin, A. Ruiz de Luzuriaga, G. Cabañero, H. J. Grande and I. Odriozola, Catalyst-free room-temperature self-healing elastomers based on aromatic disulfide metathesis, *Mater. Horiz.*, 2014, **1**, 237–240; (*b*) A. Ruiz de Luzuriaga, R. Martin, N. Markaide, A. Rekondo, G. Cabañero, J. Rodríguez and I. Odriozola, Epoxy resin with exchangeable disulfide crosslinks to obtain reprocessable, repairable and recyclable fiber-reinforced thermoset composites, *Mater. Horiz.*, 2016, **3**, 241–247.

6 (*a*) O. R. Cromwell, J. Chung and Z. Guan, Malleable and self-healing covalent polymer networks through tunable dynamic boronic ester bonds, *J. Am. Chem. Soc.*, 2015, **137**, 6492–6495; (*b*) Y. Nishimura, J. Chung, H. Muradyan and Z. Guan, Silyl ether as a robust and thermally stable dynamic covalent motif for malleable polymer design, *J. Am. Chem. Soc.*, 2017, **139**, 14881–14884.

7 (*a*) Y. Zhang, L. Tao, S. Li and Y. Wei, Synthesis of multiresponsive and dynamic chitosan-based hydrogels for controlled release of bioactive molecules, *Biomacromolecules*, 2011, **12**, 2894–2901; (*b*) G. Zhou, H. Zhang, Z. Su, X. Zhang, H. Zhou, L. Yu, C. Chen and

X. Wang, A biodegradable, waterproof, and thermally processable cellulosic bioplastic enabled by dynamic covalent modification, *Adv. Mater.*, 2023, **35**, 2301398.

8 S. Bonardd, M. Nandi, J. I. H. García, B. Maiti, A. Abramov and D. D. Díaz, Self-healing polymeric soft actuators, *Chem. Rev.*, 2023, **123**, 736–810.

9 P. Cordier, F. Tournilhac, C. Soulié-Ziakovic and L. Leibler, Self-healing and thermoreversible rubber from supramolecular assembly, *nature*, 2008, **451**, 977–980.

10 (*a*) M. Nakahata, Y. Takashima, H. Yamaguchi and A. Harada, Redox-responsive self-healing materials formed from host–guest polymers, *Nat. Commun.*, 2011, **2**, 511; (*b*) H. Wang, C. N. Zhu, H. Zeng, X. Ji, T. Xie, X. Yan, Z. L. Wu and F. Huang, Reversible ion-conducting switch in a novel single-ion supramolecular hydrogel enabled by photoresponsive host–guest molecular recognition, *Adv. Mater.*, 2019, **31**, 1807328.

11 X. Li and J. P. Gong, Role of dynamic bonds on fatigue threshold of tough hydrogels, *Proc. Natl. Acad. Sci. U.S.A.*, 2022, **119**, e2200678119.

12 (*a*) S. Burattini, B. W. Greenland, D. H. Merino, W. Weng, J. Seppala, H. M. Colquhoun, W. Hayes, M. E. Mackay, I. W. Hamley and S. J. Rowan, A healable supramolecular polymer blend based on aromatic π-π stacking and hydrogen-bonding interactions, *J. Am. Chem. Soc.*, 2010, **132**, 12051–12058; (*b*) Y. Lai, X. Kuang, W.-H. Yang, Y. Wang, P. Zhu, J.-P. Li, X. Dong and D.-J. Wang, Dynamic bonds mediate π-π interaction via phase locking effect for enhanced heat resistant thermoplastic polyurethane, *Chinese J. Polym. Sci.*, 2021, **39**, 154–163.

13 M. W. Urban, D. Davydovich, Y. Yang, T. Demir, Y. Zhang and L. Casabianca, Key-and-lock commodity self-healing copolymers, *Science*, 2018, **362**, 220–225.

14 (*a*) M. Burnworth, L. Tang, J. R. Kumpfer, A. J. Duncan, F. L. Beyer, G. L. Fiore, S. J. Rowan and C. Weder, Optically healable supramolecular polymers, *nature*, 2011, **472**, 334–337; (*b*) G. Li, J. Zhao, Z. Zhang, X. Zhao, L. Cheng, Y. Liu, Z. Guo, W. Yu and X. Yan, Robust and Dynamic Polymer Networks Enabled by Woven Crosslinks, *Angew. Chem., Int. Ed.*, 2022, **61**, e202210078.

15 (*a*) L. Chen, R. Liu and Q. Yan, Polymer Meets Frustrated Lewis Pair: Second-Generation CO2-Responsive Nanosystem for Sustainable CO2 Conversion, *Angew. Chem., Int. Ed.*, 2018, **57**, 9336–9340; (*b*) U. Yolsal, T. A. R. Horton, M. Wang and M. P. Shaver, Cyclic Ether Triggers for Polymeric Frustrated Lewis Pair Gels, *J. Am. Chem. Soc.*, 2021, **143**, 12980–12984; (*c*) T. A. R. Horton, M. Wang and M. P. Shaver, Polymeric frustrated Lewis pairs in CO2/cyclic ether coupling catalysis, *Chem. Sci.*, 2022, **13**, 3845–3850; (*d*) J. Holland, T. Horton and M. P. Shaver, Amine-Derived Polymeric Frustrated Lewis Pair Networks and Catalysts, *ACS Appl. Polym. Mater.*, 2024, **6**, 12321–12328.

16 Y. Ren and X. Dong, Dynamic polymeric materials via hydrogen-bond cross-linking: effect of multiple network topologies, *Prog. Polym. Sci.*, 2024, **158**, 101890.

17 S. H. M. Söntjens, R. P. Sijbesma, M. H. P. van Genderen and E. W. Meijer, Stability and lifetime of quadruply hydrogen bonded 2-Ureido-4[1H]-pyrimidinone dimers, *J. Am. Chem. Soc.*, 2000, **122**, 7487–7493.

18 R. G. Pearson, Hard and soft acids and bases, HSAB, part 1: fundamental principles, *J. Chem. Educ.*, 1968, **45**, 581–587.

19 R. Tepper, S. Bode, R. Geitner, M. Jäger, H. Görls, J. Vitz, B. Dietzek, M. Schmitt, J. Popp, M. D. Hager and U. S. Schubert, Polymeric halogen-bond-based donor systems showing self-healing behavior in thin films, *Angew. Chem., Int. Ed.*, 2017, **56**, 4047–4051.

20 A. H. Bui, A. D. F. Pulle, A. S. Micallef, J. J. Lessard and B. T. Tuten, Dynamic chalcogen squares for material and topological control over macromolecules, *Angew. Chem., Int. Ed.*, 2024, **63**, e202404474.

21 H. Guo, J. M. Rautiainen, H. Zeng, K. Rissanen, A. Priimagi and R. Puttreddy, Supramolecular chalcogen-bonded shape memory actuators, *Angew. Chem., Int. Ed.*, 2025, **64**, e202508101.

22 (*a*) S. Benz, A. I. Poblador-Bahamonde, N. Low-Ders and S. Matile, Catalysis with pnictogen, chalcogen, and halogen bonds, *Angew. Chem. Int. Ed.*, 2018, **57**, 5408–5412; (*b*) M. Yang, D. Tofan, C.-H. Chen, K. M. Jack and F. P. Gabbaï, Digging the sigma-hole of organoantimony lewis acids by oxidation, *Angew. Chem. Int. Ed.*, 2018, **57**, 13868–13872; (*c*) M. Yang, N. Pati, G. Bélanger-Chabot, M. Hiraia and F. P. Gabbaï, Influence of the catalyst structure in the cycloaddition of isocyanates to oxiranes promoted by tetraarylstibonium cations, *Dalton Trans.*, 2018, **47**, 11843–11850; (*d*) M. Yang, M. Hiraia and F. P. Gabbaï, Phosphonium–stibonium and bis-stibonium cations as pnictogen-bonding catalysts for the transfer hydrogenation of quinolines, *Dalton Trans.*, 2019, **48**, 6685–6689; (*e*) A. Gini, M. Paraja, B. Galmés, C. Besnard, A. I. Poblador-Bahamonde, N. Sakai, A. Frontera and S. Matile, Pnictogen-bonding catalysis: brevetoxin-type polyether cyclizations, *Chem. Sci.*, 2020, **11**, 7086–7091; (*f*) M. Paraja, A. Gini, N. Sakai and S. Matile, Pnictogen-bonding catalysis: an interactive tool to uncover unorthodox mechanisms in polyether cascade cyclizations, *Chem. Eur. J.*, 2020, **26**, 15471–15476; (*g*) J. Zhang, J. Wei, W.-Y. Ding, S. Li, S.-H. Xiang and B. Tan, Asymmetric pnictogen-bonding catalysis: transfer hydrogenation by a chiral antimony(V) cation/anion pair, *J. Am. Chem. Soc.*, 2021, **143**, 6382–6387; (*h*) H. V. Humeniuk, A. Gini, X. Hao, F. Coelho, N. Sakai and S. Matile, Pnictogen-bonding catalysis and transport combined: polyether transporters made in situ, *JACS Au*, 2021, **1**, 1588–1593; (*i*) X. Hao, T.-R. Li, H. Chen, A. Gini, X. Zhang, S. Rosset, C. Mazet, K. Tiefenbacher and S. Matile, Bioinspired ether cyclizations within a π-basic capsule compared to autocatalysis on π-acidic surfaces and pnictogen-bonding catalysts, *Chem. Eur. J.*, 2021, **27**, 12215–12223; (*j*) H. Chen, A. Frontera, M. Ángeles Gutiérrez López, N. Sakai and S. Matile, Pnictogen-bonding catalysts, compared to tetrel-bonding catalysts: more than just weak lewis acids, *Helv. Chim. Acta*, 2022, **105**, e202200119; (*k*) B. L. Murphy and

F. P. Gabbaï, Binding, sensing, and transporting anions with pnictogen bonds: the case of organoantimony lewis acids, *J. Am. Chem. Soc.*, 2023, **145**, 19458–19477; (*l*) J. E. Smith and F. P. Gabbaï, Are Ar3SbCl2 species lewis acidic? exploration of the concept and pnictogen bond catalysis using a geometrically constrained example, *Organometallics*, 2023, **42**, 240–245; (*m*) G. Renno, D. Chen, Q.-X. Zhang, R. M. Gomila, A. Frontera, N. Sakai, T. R. Ward and S. Matile, Pnictogen-bonding enzymes, *Angew. Chem., Int. Ed.*, 2024, **63**, e202411347; (*n*) G. Renno, Q.-X. Zhang, A. Frontera, N. Sakai and S. Matile, A fluorogenic substrate for quinoline reduction: pnictogen-bonding catalysis in aqueous systems, *Helv. Chim. Acta*, 2024, **107**, e202400015; (*o*) B. Zhou, S. Bedajna and F. P. Gabbaï, Pnictogen bonding at the service of gold catalysis: the case of a phosphinostiborane gold complex, *Chem. Commun.*, 2024, **60**, 192–195; (*p*) Q.-X. Zhang, G. Renno, J. J. Nué-Martinez, C. Besnard, R. M. Gomila, A. Frontera, N. Sakai and S. Matile, Pnictogen-bonding catalysis compared with ion transport in lipid bilayer membranes: entering the goldilocks inverted region, *CCS Chem.*, 2025, **7**, 91–104.

23 K. M. Bąk, S. C. Patrick, X. Li, P. D. Beer and J. J. Davis, Engineered Binding Microenvironments in Halogen Bonding Polymers for Enhanced Anion Sensing, *Angew. Chem., Int. Ed.*, 2023, **62**, e202300867.

24 (*a*) T. G. Mason and D. A. Weitz, Optical Measurements of Frequency-Dependent Linear Viscoelastic Moduli of Complex Fluids, *Phys. Rev. Lett.*, 1995, **74**, 1250; (*b*) I. Alshareedah, M. Muhammad Moosa, M. Pham, D. A. Potoyan and P. R. Banerjee, Programmable viscoelasticity in protein-RNA condensates with disordered sticker-spacer polypeptides, *Nat. Commun.*, 2021, **12**, 6620.

25 H. Lee, J. Kim, M. Lee and J. Kang, Dynamic Bond Chemistry in Soft Materials: Bridging Adaptability and Mechanical Robustness, *Chem. Rev.*, 2025, **125**, 11379–11425.

26 CCDC 2480747: Experimental Crystal Structure Determination, 2026, DOI: 10.5517/ccdc.csd.cc2p8f3j.